Segmental Dynamics in Dendrimers with Perfluorinated End Groups: A Study Using Quasielastic Neutron Scattering

B. Stark and B. Stühn*

Fakultät für Physik, Universität Freiburg, Hermann-Herder-Strasse 3, D-79104 Freiburg, Germany

H. Frey, C. Lach, and K. Lorenz

Institut für Makromolekulare Chemie, Universität Freiburg, Stefan-Meier-Strasse 21/31, D-79104 Freiburg, Germany

B. Frick

Institut Laue Langevin, F-38043 Grenoble Cedex, France

Received February 4, 1998; Revised Manuscript Received June 8, 1998

ABSTRACT: A series of carbosilane dendrimer generations, G*x*RF6 ($x = 1-3$) with perfluorohexyl ($-C_6F_{13}$) groups on the surface and one dendrimer G3 without these end groups, have been studied using X-ray scattering and quasielastic neutron scattering. The G*x*RF6 form generation dependent superstructures as a result of the microphase separation between the end groups and the carbosilane core. The helical end groups tend to arrange in layers between the carbosilane domains. The dynamic structure factor was measured with two backscattering spectrometers (IN10, IN16). For G*x*RF6 it was composed of two separable contributions referring to the segmental diffusion in the dendrimer core and the rotational diffusion of the end groups. G3 shows only one component. The segmental diffusion in the G3RF6 is reduced by a factor of 7.4 compared to G3, demonstrating the influence of the end groups on the segmental diffusion. A universal length controls the segmental diffusion of the four dendrimers. It gives rise to a characteristic scattering vector dependence of the quasielastic line width. Increasing generation number slows down the segmental diffusion and extends the lifetime of a local dynamical process. The rotational diffusion of the end groups is not strongly affected by *x*. It is less strongly dependent on temperature than the segmental diffusion.

1. Introduction

Dendrimers represent a unique class of macromolecules.[1−4] They are highly branched, three-dimensional structures emanating from a central point of functionality *f*. Linear blocks of uniform length are attached to the functional center and end again at a branching point. Each such step of growth is called a generation. The generation $g = 0$, consisting of only the branching center and *f* arms, is a star polymer. Dendrimers with core shell structure are of particular interest. In solution they represent unimolecular micelles,[5,6] which are able to solubilize and transport organic guest molecules. The segmental dynamics of such molecules in bulk is expected to differ significantly from that of linear macromolecules, which interpenetrate strongly. Whereas there has been important progress in the synthesis of these molecules,[4,7] only a few studies focus on their physical properties. In a recent publication we reported on the synthesis and the characterization of a series of carbosilane dendrimers with perfluorohexyl end groups ($-C_6F_{13}$).[8] The molecules consist of a highly flexible carbosilane core, which is unable to crystallize due to the branched structure of the dendrimer. The end groups are immiscible with the core and may be considered to be stiff rods. In bulk we therefore expect to find a microphase-separated structure with carbosilane domains separated by domains of $-C_6F_{13}$ rods. This building principle has been used in several studies of linear polymers,[9] but not for dendrimers. The resulting superstructure will reflect the compromise between the intrinsically spherical architecture of the single dendrimer molecule and the strong tendency of the end groups to form layers.

A systematic variation of the glass transition with the generation number was observed.[10] This is taken as an indication of its influence on the segmental dynamics. It is therefore important to study the segmental dynamics in a series of dendrimers with differing generation number. The major factors influencing the segmental dynamics will be shown to be the mesostructure of the system and the molecular architecture. To study this relation, dynamic measurements are combined with structural information.

In the present study we investigate the mesostructure of the carbosilane dendrimers in bulk using the full angular range of the Siemens D500 diffractometer. The domain structure, as well as the correlation of the $-C_6F_{13}$ rods in their layers are, thus, both accessible.

For the diffusive dynamics of the dendrimers quasielastic neutron scattering (QENS) is employed. This method has the advantage of providing spatial as well as time resolution unlike local methods such as fluorescence emission.[11] In the past QENS was used successfully to explore the segmental dynamics in linear, flexible polymers in solution and in the melt. For nonentangled molecules the dynamical models of Rouse and Zimm were found to be a good description of the microscopic dynamics. The dynamics of dendrimers, however, is more complex, as it involves diffusion within a highly branched, but extraordinarily well-defined, structure.[12,13]

2. Experimental Section

Three generations of a carbosilane dendrimer G1RF6, G2RF6, and G3RF6 were prepared and functionalized with $-C_6F_{13}$ groups on the surface. Their synthesis is described elsewhere.[8] Additionally, a nonfunctionalized

S0024-9297(98)00166-1 CCC: $15.00
Published on Web 07/24/1998

Table 1. Description of the Dendrimers Used in This Study

	calc mol wt	n_e[a]	n_H[b]	(R_g^2/l^2)[c]	T_g/K
G1RF6	5364.6	12	144	1.38	243
G2RF6	16315.4	36	456	2.20	234
G3RF6	49170.7	108	1392	3.18	232
G3	8112.7		852	3.18	188

[a] n_e: number of end groups. [b] n_H: number of hydrogen atoms in the dendrimer. [c] Calculated according to eq 2. The end groups are not taken into account.

dendrimer, G3, of generation 3 has been used in the neutron scattering experiments for comparison. Quantitative perfluoroalkylation of the dendrimers was demonstrated by NMR and SEC (size exclusion chromatography). Details of the molecular structure are compiled in Table 1.

For the X-ray scattering experiments Cu Kα radiation from a sealed X-ray tube was used. The wavelength is $\lambda = 0.1542$ nm. A Siemens D500 diffractometer was employed, which had been modified to perform angular and temperature scans under computer control. The scattered intensity was analyzed with a secondary monochromator, and scans were performed in $\theta-2\theta$ mode in reflection geometry. The sample was housed in an evacuated chamber. This allowed heating and cooling with a temperature stability of better than 0.5 K.

The samples were obtained from solution by evaporation of the solvent (C_6F_{14}) and filled into a rectangular sample holder. Typically, 100 mg was used for the measurement. Most measurements were done at room temperature. Special precautions had to be taken for G1RF6, which is of low viscosity at room temperature. These data were obtained after the sample was annealed at $T = 249$ K for 30 min in order to allow the ordered state to equilibrate. Subsequently, it was cooled rapidly to $T = 220$ K (below T_g). This prevented flow of the sample when the sample holder was tilted during the measurement.

The high-resolution quasielastic neutron scattering experiments were performed at the high flux reactor of the ILL, Grenoble, France. Two instruments (IN10 and IN16) were used, both of which are based on the principle of a backscattering spectrometer.[14] The incident wavelength is $\lambda = 0.6271$ nm, resulting in a range of accessible elastic scattering vectors $0.9 < q/\mathrm{nm}^{-1} < 19$. The range of energy transfer depends on the doppler frequency used in the experiment and was $-13 < \Delta E/\mu\mathrm{eV} < +13$. The energy resolution of IN16 is an improvement on the energy resolution of IN10 (see below). IN10 offers eight detectors at selected q values, whereas the same angular range is covered by two small angle detectors and a 20 channel multidetector with IN16. The samples were contained in either a hollow aluminum cylinder with a sample thickness of 0.08 mm or a flat aluminum holder with a sample thickness of 0.3 mm. It was mounted in the standard ILL cryofurnace, which allows temperature variation from 1.5 K to 600 K. The resulting transmission of the samples was larger than 0.9, and therefore multiple scattering corrections were neglected. The data were corrected for instrumental background by subtraction of a measurement using the appropriate empty sample cell. All instrumental factors influencing the intensity were eliminated by normalizing the data to the elastic scattering from an incoherent scatterer (vanadium).

3. Static Structure

The static structure factor, as determined by X-ray scattering, provides information on a wide range of length scales in our samples. A preliminary account of these results has been given in ref 8. Here we extend these results and relate the dynamic to the static structure factor. In the wide angle regime, the scattering pattern is dominated by scattering from the $-C_6F_{13}$ rods. The small angle regime, however, displays the correlation of electron density fluctuations on a length scale between 1 and 10 nm. In the first part of this section we will turn to this regime in order to characterize the superstructure of the dendrimers. We will then proceed to the structural properties on a more local scale.

The dendrimers of generation $g = 1$ to $g = 3$ differ strongly in the number of end groups per molecule. Quite generally for a branching center of functionality f and dendrimer generation g the number of end groups is $n_e = f(f-1)^g$ (see Table 1). If we accept a coarse description of the dendrimer and only count the number of branches, n_b, then

$$n_b = 1 + \frac{f((f-1)^{g+1} - 1)}{f-2} \tag{1}$$

Despite the strong variation of n_e with g the ratio between n_e and the molecular weight only decreases by 2% between $g = 1$ and $g = 3$. To obtain a measure of the unperturbed dimension of the dendrimer molecule we use a Gaussian model for the distribution of distances between the freely jointed n_b blocks. If each block is described by its mean square end-to-end distance l^2 then the radius of gyration R_g is[12]

$$R_g^2 = l^2 \frac{f(2(f-1)^{1+g}f - 1 + (f-1)^{2+2g}(1 - 4f + f^2 - 2fg + f^2g))}{(f-2)((f-1)^{1+g}f - 2)^2} \tag{2}$$

The results for R_g^2/l^2 are included in Table 1. They may serve as an estimate for the size of the unperturbed single dendrimer. We emphasize that eq 2 does not take the end groups into account. Experiments are currently in progress to determine l^2 from the single molecule size in solution. We expect l to be of the order of 2.2 nm.

In Figure 1 we compare the X-ray scattering pattern at low angles for the three dendrimers. The intensities are not on an absolute scale. The difference in mesostructure, however, is clearly visible in the figure.

For the low-temperature structure of G1RF6 we find three equidistant peaks, which indicate the existence of a layered structure. The layer spacing is 2.73(±0.05) nm, as determined from the second- and third-order reflection (see Figure 1). Closer inspection of the peak form shows a splitting of all reflections corresponding to a second period enlarged by 5%. The mesostructure suggested by this finding is a sequence of layers consisting of a $-C_6F_{13}$ double layer separated by the carbosilane core of the dendrimer. On the basis of our data, it is not possible to discriminate this model from the alternative model of a single layer of end groups with helices from both sides interdigitating. To fit into this structure the dendrimer molecule needs to adopt a flat, platelike form with the end groups protruding from both surfaces. This type of layered structure is typical for

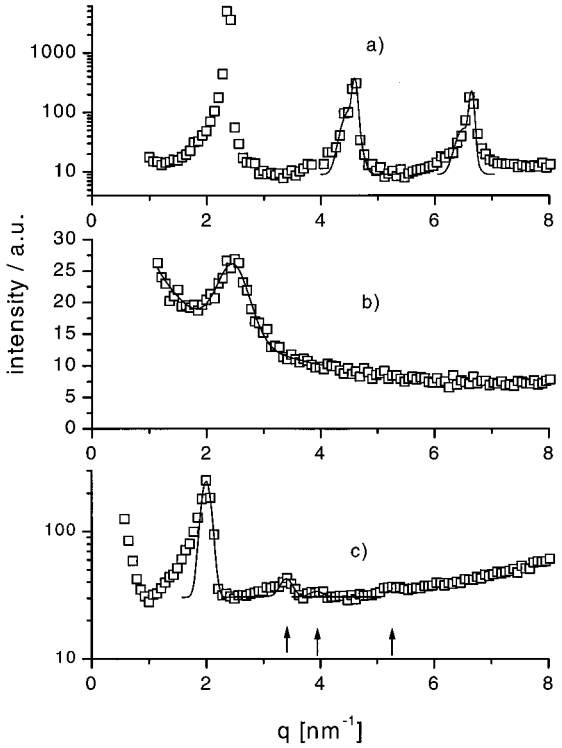

Figure 1. X-ray profiles of G1RF6 (a), G2RF6 (b), and G3RF6 (c) in the small angle range of the D500 diffractometer. The drawn lines are Gaussian fits. For G3RF6 higher order reflections are discernible (see arrows).

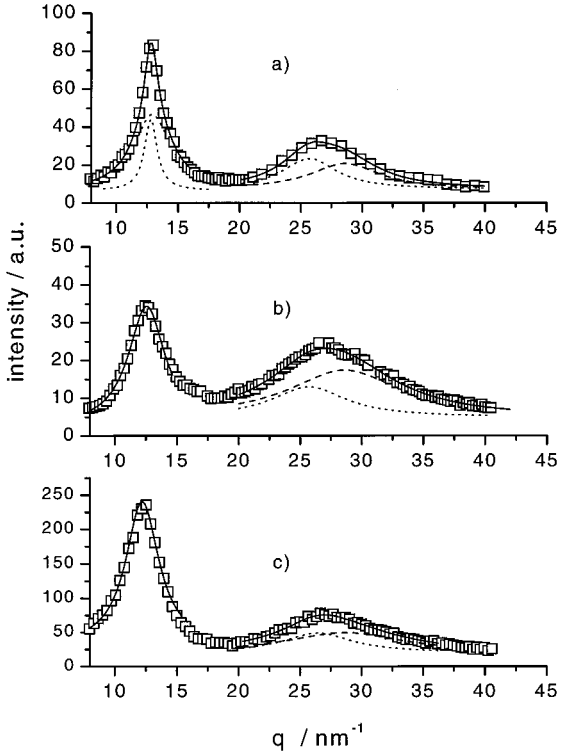

Figure 2. X-ray profiles of G1RF6 (a), G2RF6 (b), and G3RF6 (c) in the wide angle range. The general shape is similar for the three dendrimers. The drawn lines are Lorentzian fits. In the case of G1RF6 the end group interference peak is resolved into a narrow (Bragg-like) and a broad component. The peak at larger q is in the torus range of the helical structure factor and is the sum of two components (broken lines).

oligomers of perfluorinated alkanes in their crystalline state. The molecules are helices and their monomer length projected onto the long axis of the helix is $\Delta z = 0.130$ nm.[15] The interface between the helices accommodates the end standing fluorine and its thickness is found to be 0.23 nm. Assuming a similar packing density the double layer in the case of G1RF6 would therefore amount to 1.79 nm leaving a thickness of 0.94 nm for the carbosilane core. The peak splitting (see Figure 1) indicates the possible existence of a tilted orientation of the $-C_6F_{13}$ in their layers in some domains of the sample. This arises as a result of the nonperfect packing in lateral direction.

The mesostructure of G2RF6 is not well-defined, as is seen in Figure 1b. There is only one broad peak at $q = 2.47(\pm 0.04)$ nm^{-1}. This is larger than the position of the first-order reflection of G1RF6. It corresponds to a length of $r = 2.54$ nm for the distance between carbosilane domains. The increased size of the dendrimer core and the increased density of the end groups with respect to G1RF6 no longer allows the formation of the lamellar order. The lateral extent of the lamellae is limited by the size of the dendrimer core, and no long range order can be built up. Consequently, we do not find higher order reflections. If we use the same thickness for the $-C_6F_{13}$ double layer, then the remaining size for the carbosilane core is only 0.68 nm. A different type of order is therefore suggested, which is similar to that of G3RF6.

The even larger size of G3RF6 then enables the formation of a new type of mesostructure, as is seen in Figure 1c. The strong peak at q_1 is now followed by weak higher order reflections at positions $q_2 = \sqrt{3}q_1$, $q_3 = \sqrt{4}q_1$, and $q_4 = \sqrt{7}q_1$. This is in accordance with the assumption of cylindrical domains arranged on a hexagonal lattice. The distance d_{cyl} between the cylinders may be derived from the value of $q_1 = 4\pi/(d_{cyl}\sqrt{3})$ as $d_{cyl} = 3.66(\pm 0.06)$ nm. Assuming the same, but less well ordered, superstructure for G2RF6, the corresponding distance of cylinders is 2.9 nm. The ratio of d_{cyl} for the two samples is approximately the same as the calculated ratio of the radii of gyration for G3RF6 and G2RF6, as given in Table 1. The local order in both systems may therefore be taken to be the same.

This conclusion is confirmed by the X-ray scattering data at larger q, as shown in Figure 2. All samples exhibit two peaks in this regime. The first peak is the result of the interference between scattering from the $-C_6F_{13}$ end groups, whereas the second maximum will be shown to result mainly from their internal structure. As in the case of the small angle scattering pattern, a clear difference is observed between G1RF6 on one side and G2RF6 and G3RF6 on the other side. The peak shape for the latter is Lorentzian, indicating only short range order, whereas for G1RF6 a narrow component is superimposed (see Figure 2). The end groups are arranged in a crystalline order within their layers. Assuming a hexagonal packing with an end group distance a, we assign the narrow peak to the {100} reflection. Its center is at $q_{100} = 12.81$ nm^{-1}, resulting in an end group distance $a = 0.57$ nm. This value is in agreement with the result of ref 15 for the lattice constant of perfluoro-*n*-eicosane in "phase R". The well-developed layers in G1RF6 enable lateral order of the $-C_6F_{13}$ just as in the oligomer crystal. Consequently, the peak consists of a narrow Bragg type reflection on top of a diffuse scattering component (see Figure 2). No three-dimensional crystalline order can build up, as the correlation perpendicular to the layers can only extend

over two layers. The cylindrical domain structure of G2RF6 and G3RF6 prevents the formation of long range order between the end groups. Consequently, the corresponding reflection does not contain a narrow Bragg peak. As shown in Figure 2 the peak maximum is below q_{100} of G1RF6 because the average end group distance is increased.

The second peak displayed in the scattering patterns of Figure 2 does not show significant difference in shape or position for the three dendrimer generations. Its intensity is comparable to that of the end group interference peak. It is the result of correlation in the internal structure of the $-C_6F_{13}$ groups. Perfluorinated alkanes in their crystalline state are of helical structure. The form factor of a single helix, consisting of carbon (C) and fluorine (F) atoms, gives rise to a characteristic scattering pattern.[16] The periodic sequence of scatterers along the helix axis, with a periodicity Δz in combination with the cylindrical symmetry, results in two adjacent maxima, which for a single helix are of toroidal shape in reciprocal space. Due to the finite length of the $-C_6F_{13}$ groups and the orientational averaging, this results in two smeared out peaks. The full lines in Figure 2 are fits with two Lorentzian-shaped maxima centered at $q_{tor,1} = 25.7\ nm^{-1}$ and $q_{tor,2} = 28.6\ nm^{-1}$. These values would be expected for a 15/7-helix with $\Delta z = 0.13$ nm. Our data are consistent with these parameters.

4. Segmental Dynamics

In this section we present the results of QENS from the four dendrimers in bulk. We briefly recall the relevant relations between the dynamic structure factor as measured with QENS and the microscopic dynamics. We then describe the procedure used in the data analysis before discussing the results.

A. Dynamic Structure Factor. The regime of scattering vectors q covered by the backscattering instruments, IN10 and IN16, is nearly identical and extends from the small q shown in Figure 1 up to $q = 18.9\ nm^{-1}$ in Figure 2. The experiment therefore is able to probe the relaxational dynamics on length scales between the end group distance and the mesoscopic lattice parameters. In general, the scattering intensity per molecule is the sum of the incoherent and the coherent scattering.[17]

$$I(q,\omega) \propto n_H \sigma_{inc} S_{inc}(q,\omega) + n_e \sigma_{coh} S_{coh}(q,\omega) \qquad (3)$$

$S_{coh}(q,\omega)$ and $S_{inc}(q,\omega)$ denote the coherent and the incoherent scattering function. The frequency ω is related to the energy transfer in the scattering process $\Delta E = \hbar\omega$. The change in the wavelength of the neutron in the scattering process does not lead to a significant change of q, which is expressed as the quasielastic approximation.

In the present case, the incoherent and the coherent parts also separate scattering from the dendrimer core from that of its end groups. The incoherent scattering component is almost exclusively caused by the scattering from hydrogen and therefore refers to the dendrimer core. We let n_H be the number of hydrogen atoms in the core and $\sigma_{inc} = 79.9 \times 10^{-28}\ m^2$ the incoherent cross section per hydrogen. Values for n_H are given in Table 1. The coherent scattering on the other side is mainly caused by carbon and fluorine and may be considered to be dominated by the n_e helical end groups (Table 1) of the dendrimer. In eq 3 we assume that there is no correlation in the motion of neighboring end groups. The coherent intensity varies with q according to the scattering function. The X-ray scattering profiles may be taken to be approximately proportional to the static coherent scattering, i.e., the integrated coherent scattering function, because it is also dominated by the scattering from carbon and fluorine.

In general, the integral with respect to ω of the incoherent scattering contribution is independent of q. A spectrometer with finite resolution, however, does not resolve fast dynamical processes, which then give rise to a Debye−Waller factor (see below). For the present case the spectrometer resolves the long range diffusion of segments of the macromolecule and the distribution of hydrogen atoms may be assumed to be Gaussian:

$$S_{inc}(q,\omega) = \frac{1}{2\pi\hbar}\int_{-\infty}^{\infty} dt\ e^{-i\omega t} \frac{1}{n_H}\sum_j \exp\left(-\frac{q^2}{6}\langle(\vec{r}_j(0) - \vec{r}_j(t))^2\rangle\right) \qquad (4)$$

The sum in eq 4 extends over all hydrogens in the dendrimer. It is evident from eq 4 that the incoherent scattering allows determination of the time dependence of the mean-squared displacement of the average hydrogen in the dendrimer. For a freely diffusing particle, the Einstein relation holds and relates the mean-squared displacement of the scatterer to the diffusion coefficient D: $\langle(\vec{r}_j(0) - \vec{r}_j(t))^2\rangle = 6Dt$. Fourier transformation then yields the well-known result[14]

$$S_{inc}(q,\omega)_{FD} = \frac{1}{\pi}\frac{Dq^2}{\omega^2 + (Dq^2)^2} \qquad (5)$$

The scattering law is a single Lorentzian line with a full width at half-maximum (fwhm) of $2Dq^2$. In units of frequency we denote the fwhm as $\Delta\omega$. Measurement of the fwhm of the scattering function therefore enables us to determine the diffusion coefficient D.

The internal diffusion of linear polymer chains gives rise to a superposition of lines of the form of eq 5 corresponding to the relaxational modes that contribute at a given scattering vector q. The form of $S_{inc}(q,\omega)$ and $S_{coh}(q,\omega)$ is known explicitly[18,19] for the cases of negligible or dominant hydrodynamic interaction. In contrast to eq 5 the characteristic frequency as determined as the fwhm shows an even stronger dependence on q. The present case of a highly branched structure is closer to the situation of a polymer network. Here the diffusion of the average hydrogen is confined to the volume between branching points as described by a confinement length ξ. The scattering law is of the form given by eq 5 as long as $q\xi > 1$. For smaller q an elastic contribution to the scattering would be expected as a result of the confinement.

Turning to the coherent scattering from the end groups of the dendrimer, we are guided by the results reported in refs 20−24 concerning the dynamics of the perfluorinated oligomer $C_{20}F_{42}$ in its crystalline state. The crystalline structure is characterized by layers of the rodlike molecules with their long axis perpendicular to the plane. The dynamics of the molecules is a nearly free rotational diffusion around this axis. Correlation between the reorientation of the molecules is observed on approaching the low-temperature phase with alternating right- and left-handed helices. As shown above,

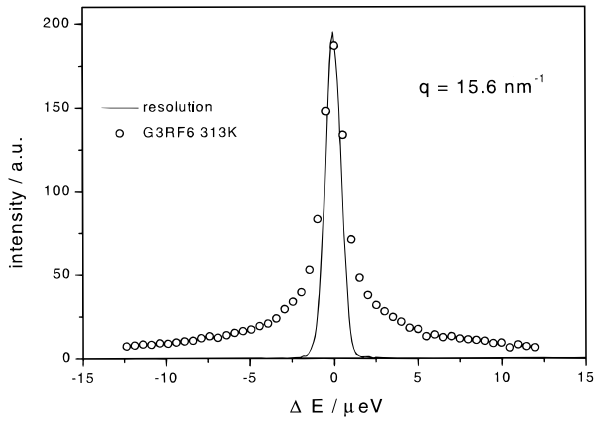

Figure 3. Typical spectrum obtained on IN16 for sample G3RF6 at $T = 313$ K. Statistical errors are of the size of the symbols. At the high q shown in the figure the broadening of the inner line with respect to the resolution function (drawn curve) is clearly visible.

in the present case we have only short range lateral order between the end groups for G2RF6 and G3RF6. Only G1RF6 exhibits an indication for crystalline type, long range, lateral order. The assumption of individual rotational diffusion without correlation between neighbors is therefore justified. In this situation the scattering law reflects only the dynamics of the azimuthal angle ϕ describing the orientation of the molecule with respect to rotation around its long axis. The intermediate scattering law is then[23]

$$I(q,t) \propto I_1{}^2 h^2 \exp(-D_r t) \qquad (6)$$

D_r is the rotational diffusion coefficient and it is assumed in eq 6 that the first-order Bessel function contribution is dominant in the regime of q values investigated. The q dependence is only seen in the prefactors $I_1 h$, which contain the detailed structure of the molecule. They are defined in ref 23. In our case, of a powderlike arrangement of layers, we do not insist on the details of this dependence and only note that a maximum would be expected at the location of the so-called torus at $q_t \approx 25.7$ nm^{-1}. Fourier transformation of eq 6 then yields an expression of the form of eq 5, again with the important difference that the fwhm of the Lorentzian is independent of q and given as D_r.

With these ideas in mind we expect the experimental scattering function to be the sum of two Lorentzian lines with fwhm that depend on q in a distinctly different way.

B. Reduction of Data. The experimentally determined scattering function $S_{exp}(q,\omega)$ is the convolution of the resolution of the spectrometer $R(q,\omega)$ and the theoretical scattering law, as discussed in the previous section.

$$S_{exp}(q,\omega) = \int_{-\infty}^{\infty} R(q,\omega-\omega')\, S(q,\omega')\, d\omega' \qquad (7)$$

An example of the quality of data obtained on IN16 is shown in a spectrum of sample G3RF6 at $q = 15.6$ nm^{-1} in Figure 3. The figure also includes the resolution function as a full line. It was determined with the sample at low temperature ($T = 2$ K) as an elastic scatterer. The fwhm of the resolution function is 1.05 μeV. It shows only a weak dependence on q. The form of $R(\omega)$ is nearly Gaussian. The fwhm of $S(q,\omega)$ is seen in Figure 3 as the broadening of the experimental

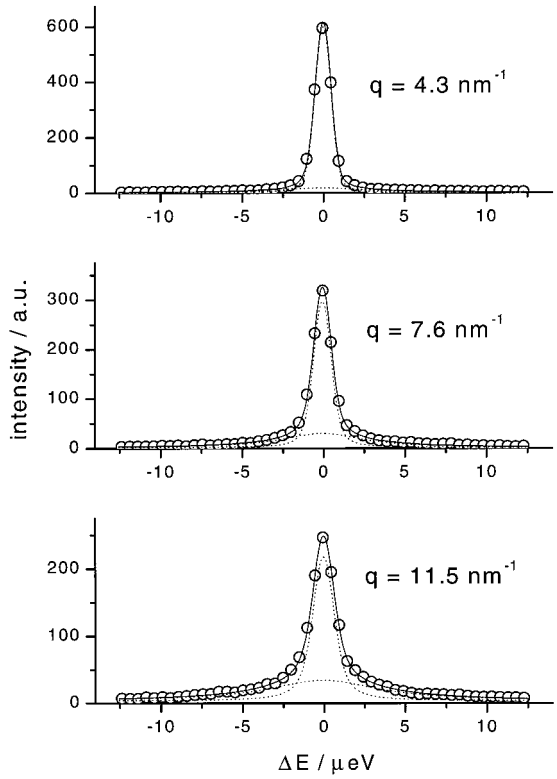

Figure 4. Change of the dynamic structure factor with q^2 for sample G1RF6 at $T = 313$ K. The lines are fits with the two-component model described in the text. As can be seen in the figure, the *broad* component does not change significantly with q whereas the *narrow* component broadens and decreases in intensity.

spectrum with respect to the resolution. To extract this information quantitatively from the data, we model $S(q,\omega)$ as described in the previous section and convolute this function numerically with the resolution function. The parameters contained in $S(q,\omega)$ are then determined at each q in a least squares procedure. In the fitting procedure it is preferable to use the full resolution function in place of the fitted Gaussian. In this way one takes its detailed form into account, which is essential when trying to decompose the scattering function into two lines.

The same method is applied to the data obtained on IN10. The resolution function of this instrument is not so ideally Gaussian as in the case of IN16 and exhibits a fwhm of 1.46 μeV.

To account for the remaining background after subtraction of the scattering from an empty sample cell, we include a flat background in the fit procedure. This accounts for fast relaxational processes that are wider than the spectral range of the spectrometer.

The spectrum shown in Figure 3 clearly cannot be described by a single Lorentzian line as the intensity in the wings decays too slowly with ω. In Figure 4 we show fits of three spectra of G1RF6 at other q using two Lorentzians, as discussed in the previous section. By this method we obtain a very good fit of the data, as is demonstrated by the full lines in the figure. The broken lines represent the separate Lorentzians, both convoluted with the resolution function. The fwhm of both components differ significantly, which is an important prerequisite for the applicability of this method.

C. Results and Discussion. At $T = 2$ K the dendrimers represent elastic scatterers. With increas-

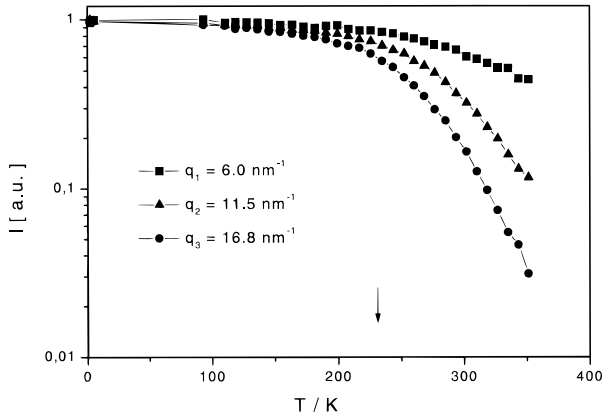

Figure 5. Elastically scattered intensity for three q values dependent on temperature. The data are for sample G3RF6 and were obtained on IN10. The glass transition temperature is marked in the plot.

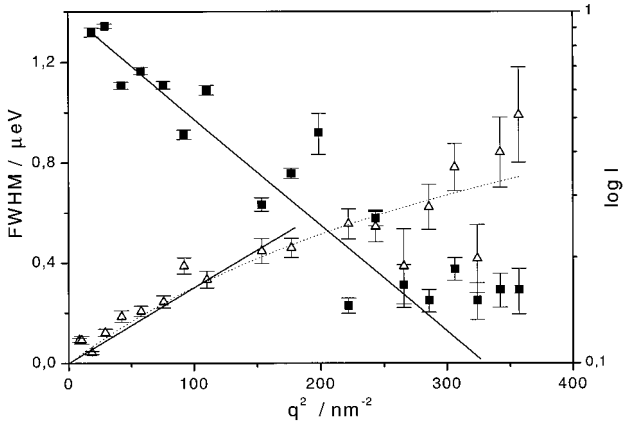

Figure 6. Variation of the *narrow* component with q^2 at T = 313 K. Left axis (open symbols): fwhm. The dotted line is a fit of the crossover formula (see text). The segmental diffusion coefficient is obtained from the straight line at small q. Right axis (filled symbols): intensity on logarithmic scale. The linear decrease is caused by a Debye−Waller factor.

ing temperature the molecular dynamics, oscillatory or diffusive in character, are enhanced, which leads to a broadening of the scattering function and correspondingly to a loss of the elastically scattered intensity. We have therefore performed an "elastic window scan" of the three samples GxRF6 with the spectrometer set to elastic scattering condition and registered the intensity at each q with temperature increasing linearly with time. The heating rate used in these measurements was 0.45 K/min. The result for G3RF6 is shown in Figure 5 for three selected q values. The data were obtained on IN10. The intensity is normalized to its value at the lowest temperature.

$q_1 = 6.0$ nm^{-1} (Figure 5) is below and $q_3 = 16.8$ nm^{-1} is above the helix−helix interference maximum (cf. Figure 2). The scattered intensity is, therefore, mainly due to the incoherent scattering from the dendrimer core. The much stronger decrease of the elastically scattered intensity at q_3 compared to that at q_1 is already a clear indication for the q dependence of the dynamics. Between 5 and 200 K only a weak decrease caused by dynamics that lies outside the spectral range of IN10 is observed. The approximately linear decrease on logarithmic scale is characteristic for a phonon type motion with the mean-squared displacement of the scatterer increasing linearly with T. Around the glass transition temperature ≈240 K, however, a strong decrease of the elastically scattered intensity is found, which is accompanied by a broadening of the scattering function. In this temperature regime the onset of a rather slow dynamics leads to a broadening that is observed within the spectral range of the instrument.

Similar behavior is found for the case of $q_2 = 11.5$ nm^{-1} covering the end group interference peak (cf. Figure 2). We emphasize the low angular resolution of the backscattering spectrometer, which covers the range of $10.1 < q/\text{nm}^{-1} < 14.4$ for the detector at q_2 used in Figure 5. The intensity collected in this detector is mainly related to the coherent scattering from the $-C_6F_{13}$ groups. The considerably slower decrease of intensity with T for this q compared to q_3 is an indication of the presence of two different dynamic processes in the dendrimer. The decomposition of the spectra at each q will be shown to identify the two processes involved in the segmental dynamics of the dendrimer molecule and to determine their separate temperature dependence.

The data shown in Figure 5 may also be used to select a temperature at which the dynamics of the dendrimers are most conveniently studied with the backscattering spectrometer. At T = 313 K we find the quasielastic broadening to be well resolved and an example is given in Figure 4. For G1RF6, G2RF6, and G3RF6 the spectra are all unambiguously described as the sum of two Lorentzian lines. In the following we refer to these components as the *narrow* and the *broad* line.

The scattering function of the dendrimer without $-C_6F_{13}$ end groups, G3, shows only one Lorentzian line. This is in support of our interpretation of the spectra obtained for the end group functionalized dendrimers.

In Figure 6 we display the parameters characterizing the q dependence of the *narrow* line for G3RF6 as measured using IN16. The fwhm is seen to show a pronounced q dependence. For $q \leq 12$ nm^{-1} it is approximated by the power law $\Delta\omega = D_{app}q^2$ and enables the determination of a monomeric diffusion coefficient. This quantity is a measure of the local chain stiffness, as has been shown for the case of linear polymer chains in the melt.[25] The universal regime of Rouse relaxation is expected to be attained at the smallest q in our experiment.

At larger q the fwhm is less strongly dependent on the scattering vector. It apparently tends to a constant value. The crossover from translational diffusion to a local relaxation occurs around $q_c \approx 13$ nm^{-1}, which corresponds to a typical segment length $b_c \approx 2\pi/q_c = 0.5$ nm. Microscopically, the crossover from diffusive behavior at small q to a q independent fwhm at large q may be understood in analogy to the model of Singwi and Sjölander.[14,26] The hydrogen executes a local, oscillatory motion for a time τ_0. τ_0 is the lifetime of the local process. At longer times the hydrogen diffuses with a diffusion coefficient D. In the limit of large τ_0 the resulting scattering law is a Lorentzian with a fwhm

$$\Delta\omega\tau_0 = 2\frac{q^2D\tau_0}{1 + q^2D\tau_0} \tag{8}$$

As is shown by the broken line in Figure 6, we can describe very well the crossover using eq 8. The initially linear increase of the fwhm with q^2 determines D and the plateau at large q is $2/\tau_0$. The parameters derived

Table 2. Diffusion Coefficient and Relaxation Time τ_0 for the Dendrimers at $T = 313$ K[a]

	$D/10^{-12}$ m^2 s^{-1}	$\tau_0/10^{-10}$ s
G1RF6	6.3 (2)	4.6 (2)
G2RF6	5.0 (0.7)	5.8[b]
G3RF6	3.2 (0.8)	9.2 (3.2)
G3	23.7 (3)	1.2 (0.2)

[a] Errors are given in parentheses. [b] For G2RF6 the common fit of D and τ_0 was unstable due to the small number of data points. τ_0 was kept fixed for the error analysis.

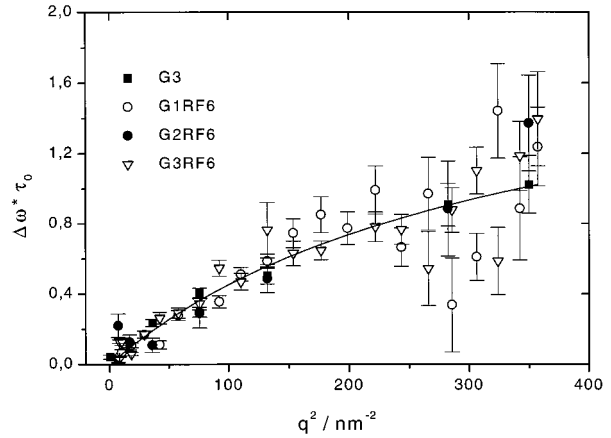

Figure 7. fwhm of all dendrimers at $T = 313$ K multiplied by τ_0. The data were obtained on IN10 (filled symbols) and IN16 (open symbols). They fall on a universal curve defining l_s^2 according to eq 8.

from these fits are given in Table 2. We observe from these values that the product $D\tau_0$ is the same for the four dendrimers. This observation is visualized by plotting the scaled fwhm as $\Delta\omega\tau_0$ according to eq 8 in Figure 7. Indeed, all data fall on one universal curve, which may now be used to determine the universal length $l_s^2 = 6D\tau_0$. It is found to be $l_s^2 = 1.74$ Å^2. The increase of dendrimer generation number slows down the long time diffusion and extends the lifetime of the local process.

The intensity I_{narrow} of this component is also shown in Figure 6 and decreases strongly with q: $I_{\text{narrow}} \propto \exp(-q^2\langle u^2\rangle/3)$. This allows us to determine the mean-squared displacement $\langle u^2\rangle$ of the scatterer caused by dynamical processes that are not resolved by the instrument. These may be the oscillatory motions mentioned above or other fast quasielastic processes that do not contribute to the long time diffusion. No further q dependence is found in the intensity of this component. The value of $\langle u^2\rangle$ is 2.4(±0.4) Å^2 for G3RF6 at 313 K. It is of the same size as l_s^2.

A different scenario is observed for the broad line of the experimental scattering function. In Figure 8 we display the fwhm and intensity for all q. As opposed to the narrow line, we find only a weak variation of the fwhm with q. It remains essentially constant and increases only by about 10% starting around the q -position of the helix−helix interference maximum (arrow in Figure 8). This is in accordance with the assumption of rotational diffusion of the helical molecule (eq 6), and the corresponding fwhm is therefore $D_r\hbar$. Quite generally, the scattering function for a helical molecule undergoing rotational diffusion is determined by the correlation of the azimuthal angle ϕ for each scattering atom. The increase of the fwhm with q may be caused by the contribution of defects to the rotational diffusion.[24] Also shown in Figure 8 is the intensity I_{broad}

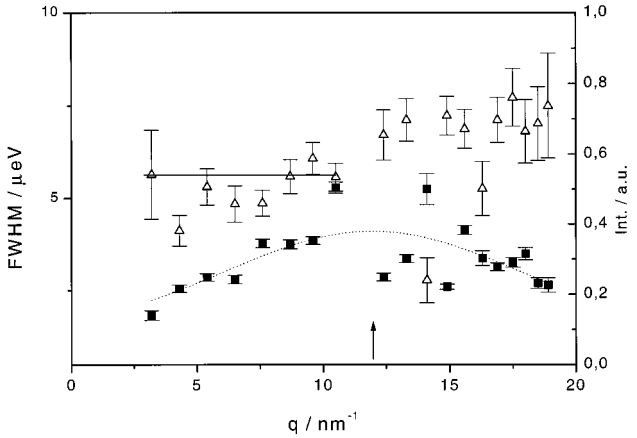

Figure 8. Variation of the *broad* component with q. Left axis (open symbols): The fwhm is nearly independent of q. The rotational diffusion coefficient is determined from the horizontal line. Right axis (filled symbols): The intensity of this component peaks at the location of the helix−helix interference peak. The dotted line is a Gaussian fit.

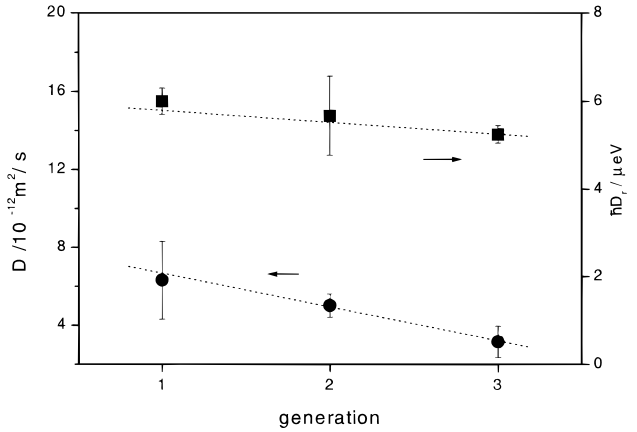

Figure 9. Variation of segmental (left axis, circles) and rotational diffusion (right axis, squares) with dendrimer generation. The lines are guidelines for the eye.

of this line. As opposed to the intensity of the slow component, it increases, with q reaching a maximum around the position of the helix−helix interference maximum in Figure 2. This confirms the assignment of this component to the coherent scattering from the helical end groups of the dendrimer. As mentionend above, dendrimer G3 (see table) without end groups does not exhibit the two-component line shape shown in Figure 4. In this case only one Lorentzian line is observed, which has the characteristics described for the *narrow* line. The *broad* component is absent, as we would expect because the helical end groups are not present in this molecule.

We can now discuss the variation of segmental and rotational diffusion with the generation of the dendrimer. These two quantities are shown in Figure 9. The segmental diffusion coefficient decreases strongly with generation by a factor of nearly 2. For the three samples with end groups it is significantly smaller than for G3, for which we find $D = 23.7(\pm2.5) \times 10^{-12}$ m^2/s. The core−shell structure of the dendrimers strongly modifies the segmental diffusion of the core part. The major factor here will be the microphase separation between the end groups and the carbosilane core, which should change the local density and therefore the effective friction coefficient of a segment. The tendency of the $-C_6F_{13}$ groups to form layers was shown to be a

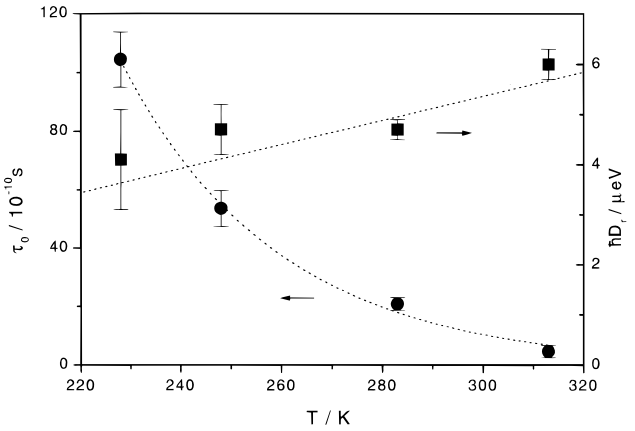

Figure 10. Temperature dependence of the lifetime τ_0 (circles) and the rotational diffusion coefficient $\hbar D_r$ (squares) for G1RF6. The dotted lines are guidelines for the eye.

determining factor for superstructure formation and correspondingly to cause a deformation of the dendrimer core. This will in turn change the flexibility of the chain segments and consequently the diffusion coefficient.

The second quantity shown in Figure 9 is the rotational diffusion coefficient as $\hbar D_r$. Its decrease with generation is much smaller than that of the segmental diffusion coefficient. The packing of the $-C_6F_{13}$ groups does not vary strongly between the three samples, as was shown above, and the observed diffusion coefficient is mainly a property of a single helix. The decrease seen in Figure 9 must therefore mainly be attributed to a coupling of the rotational diffusion to the dynamics of the dendrimer core.

Finally, we turn to the temperature dependence of the segmental dynamics in dendrimers. In Figure 10 we display the rotational diffusion coefficient $\hbar D_r$ for the example of G1RF6 in the temperature range from 228 to 313 K. The variation with T is smaller than that found in the crystal of $C_{20}F_{42}$[23] just above the transition to the rhombohedral lattice. In the latter case the loss of correlation with T adds to the temperature dependence whereas the end groups of the dendrimer perform a nearly uncorrelated rotational diffusion.

The translational diffusion is characterized by the lifetime τ_0 of the local process and shown in the same plot. It depends much more strongly on T than the rotational diffusion of the end groups: τ_0 decreases by a factor of 30 as the temperature is increased by 85 K.

At the same time the system supports dynamical processes that are faster than the resolution of the backscattering instrument. We observe these only as a decrease of the intensity in the quasielastic spectrum. As described above, we derive from the scattering vector dependence of the intensity a mean-squared displacement $\langle u^2 \rangle$, which varies strongly with temperature above T_g. These data are shown in Figure 11 for G1RF6 and G3RF6. A similar observation has been made for the case of a linear polymer (polyethylene)[27] but is considered to be a general feature of the glass transition.[28] At low temperature the results for both samples agree. The deviation at high T may be caused by the better resolution of IN16 with respect to IN10.

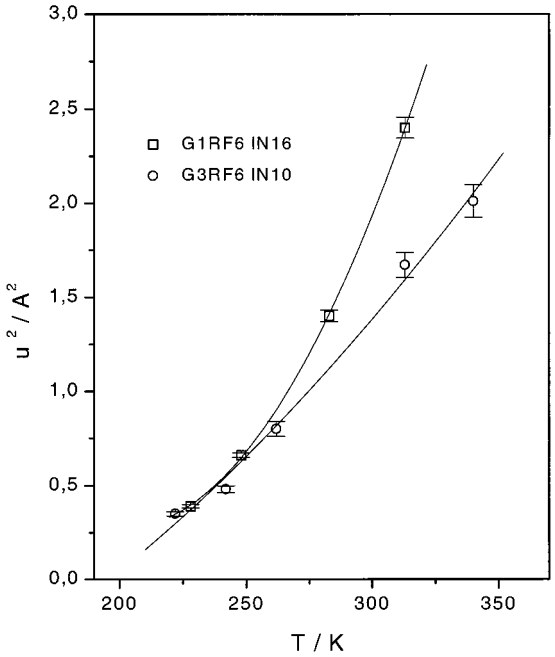

Figure 11. Mean-squared displacement $\langle u^2 \rangle$ as obtained from the Debye−Waller factor of the segmental diffusion for G1RF6, IN16 (squares) and G3RF6, IN10 (circles). The lines are guidelines for the eye.

5. Conclusions

Carbosilane dendrimers of generations 1−3 with perfluorinated end groups exhibit a superstructure that is the result of the compromise between the isotropic structure of the molecule and the tendency of the end groups to form layers. The local order within these layers is similar to that found in the crystalline state of perfluorinated alkanes. In the case of G1RF6 the layers are flat and packed in stacks but they are curved in the case of the larger molecules G2RF6 and G3RF6. As a result, in all cases the dendrimer core is deformed by the ordering of the end groups. Segmental dynamics, as studied with quasielastic neutron scattering, has shown that the demixing of end groups and the dendrimer core also leads to a dynamic heterogeneity. Due to the intrinsic labeling of the dendrimers the rotational diffusion of the end groups and the translational diffusion of the segments in the dendrimer core could be observed separately. Within the q range of the backscattering spectrometers IN10 and IN16, one probes the flexibility of the chain segments in the dendrimer. Recent theoretical work[13] has treated the Rouse dynamics of a dendrimer model. Although the dynamic structure factor is not calculated, the authors estimate the relaxation time for internal elastic motions of the dendrimer $\tau_e = 2^{g+1}\zeta/k$. ζ/k is the ratio of the segmental friction coefficient and the spring constant, which determines the time scale of relaxation in a Rouse model. The increase of τ_e with generation number g would be even stronger than we find here. We emphasize, however, that the theory applies to the universal regime of scattering vectors, which our data only reach for the smallest q. Both dynamical processes show distinctly different temperature dependences. The glass transition that is found in these materials with conventional DSC measurements shows up in the abnormal Debye−Waller factor but does not influence the local diffusive dynamics.

Acknowledgment. This work was supported by the BMBF (project number 03-ST4FRU-0). C.L. and K.L. gratefully acknowledge financial support by Fonds der chem. Industrie.

References and Notes

(1) Newkome, G. *Advances in Dendritic Macromolecules*; JAI Press Series; JAI Press: JAI Press: Greenwich, CT, 1995; Vol. 2.
(2) Newkome, G.; Moorefield, C.; V gtle, F. *Dendritic Molecules—Concepts, Synthesis, Perspectives*; Verlag Chemie: Weinheim, New York, 1996.
(3) Newkome, G. R.; Moorefield, C.; Baker, G.; Johnson, A.; Behera, R. *Angew. Chem.* **1991**, *103*, 1205.
(4) Tomalia, D. A.; Durst, H. *Top. Curr. Chem.* **1993**, *165*, 193.
(5) Newkome, G.; Yao, Z.; Baker, G.; Gupta, V. *J. Org. Chem.* **1985**, *90*, 2003.
(6) Jansen, J.; van-den Berg, E. B.; Meijer, E. *Science* **1994**, *266*, 1226.
(7) Frey, H.; Lach, C.; Lorenz, K. *Adv. Mater.*, in press.
(8) Lorenz, K.; Frey, H.; Stühn, B.; Mülhaupt, R. *Macromolecules* **1997**, *30*, 6860.
(9) Napoli, M. *J. Fluorine Chem.* **1996**, *79*, 59.
(10) Stutz, H. *J. Polym. Sci., B: Polym. Phys.* **1995**, *33*, 333.
(11) Wilken, R.; Adams, J. *Macromol. Rapid Commun.* **1997**, *18*, 659.
(12) LaFerla, R. *J. Chem. Phys.* **1997**, *106*, 688.
(13) Cai, C.; Chen, Z. *Macromolecules* **1997**, *30*, 5104.
(14) Bee, M. *Quasielastic neutron scattering;* Adam Hilger: Bristol and Philadelphia **,** 1988.
(15) Schwickert, H.; Strobl, G.; Kimmig, M. *J. Chem. Phys.* **1991,** *95*, 2800.
(16) Alexander, L. E. *X-ray diffraction methods in polymer science*' Wiley: New York, 1969; Chapter 6.
(17) Lovesey, S. W. *Theory of neutron scattering from condensed matter;* Clarendon Press: Oxford, U.K., 1987.
(18) de Gennes, P. *Physics* **1967**, *3*, 37.
(19) Dubois-Violette, E.; de Gennes, P. *Physics* **1967**, *3*, 181.
(20) Albrecht, T.; Elben, H.; Jaeger, R.; Kimmig, M.; Steiner, R.; Strobl, G.; Stühn, B.; Schwickert, H.; Ritter, C. *J. Chem. Phys.* **1991**, *95*, 2807.
(21) Albrecht, T.; Jaeger, R.; Petry, W.; Steiner, R.; Strobl, G.; Stühn, B. *J. Chem. Phys.* **1991**, 95, 2817.
(22) Albrecht, T.; Elben, H.; Jaeger, R.; Kimmig, M.; Petry, W.; Ritter, C.; Schwickert, H.; Strobl, G.; Stühn, B. *Prog. Colloid Polym. Sci.* **1992**, *87*, 46.
(23) Kimmig, M.; Steiner, R.; Strobl, G.; Stühn, B. *J. Chem. Phys.* **1993**, *99*, 8105.
(24) Kimmig, M.; Strobl, G.; Stühn, B. *Macromolecules* **1994**, *27*, 2481.
(25) Stühn, B.; Ewen, B.; Richter, D. *Z. Phys. B: Condens. Matter* **1985**, *58*, 305.
(26) Singwi, K. S.; Sjolander, A. *Phys. Rev.* **1960**, *119*, 863.
(27) Holzer, B.; Strobl, G.; Stühn, B.; Andersen, N. *Colloid Polym. Sci.* **1994**, *272*, 1396.
(28) Frick, B.; Richter, D. *Phys. Rev. B* **1993**, *47*, 14795.

MA9801669